Harnessing Valerolactone: Green and LowToxic Solvent for Enhanced DyeSensitized Solar Cells Performance Under Indoor Lighting

ADVANCED ENERGY & SUSTAINABILITY RESEARCH
www.advenergysustres.com

Harnessing γ-Valerolactone: Green and Low-Toxic Solvent for Enhanced Dye-Sensitized Solar Cells Performance Under Indoor Lighting

Roberto Speranza, Serena Amenta, Pietro Zaccagnini, Candido Fabrizio Pirri, and Andrea Lamberti*

A significant portion of the billions of Internet of Things (IoT) smart devices operate indoors, typically powered by batteries that require periodic recharging or disposal, raising sustainability concerns about maintenance and electronic waste production. This has generated increased interest in developing indoor photovoltaics (IPV) for self-rechargeable IoT devices. Among IPV technologies, dye-sensitized solar cells (DSSCs) offer high conversion efficiency, stability, and scalability. However, the use of toxic and flammable solvents, such as acetonitrile (ACN) and 3-methoxypropionitrile (MPN), remains a concern. This research investigates γ-valerolactone (γ-VL), a sustainable, low-toxic solvent derived from cellulosic biomass, as an alternative for DSSC electrolytes. Electrolytes based on I^-/I_3^- redox shuttle are prepared with γ-VL, MPN, and ACN and studied in both dummy cell and full device configuration. Results show that γ-VL is unsuitable for outdoor DSSCs due to slower ion diffusion and reduced I_3^- reduction at the counter electrode. However, γ-VL DSSCs outperform those using ACN and MPN under indoor light, demonstrating equivalent short-circuit currents but higher open-circuit voltages, improved fill factors, and enhanced overall efficiency, enabled by lower recombination at the photoanode. These findings position γ-VL as a promising, eco-friendly option for DSSC electrolytes in indoor IoT applications.

1. Introduction

One of the most distinguishing features of contemporary society is the deep interconnectedness of various elements and systems. With the exception of a few isolated cases, virtually all aspects of life—ranging from technology and communication to economics and social interactions—are interlinked. A very representative manifestation of this feature is the Internet of Things (IoT), which is none other than a network of "smart" objects, which are able to collect, process, and exchange information between each other over the internet.[1–3] Many of these objects are equipped with sensors that monitor specific variables, such as temperature, humidity, or movement, and subsequently transmit this data for analysis. By leveraging this information, it is possible to enhance the quality of our daily lives and improve the efficiency of various business operations.[3] A significant portion of the billions of new IoT devices expected to be installed in the coming years will be located in indoor environments.[4,5] Currently, most autonomous IoT nodes rely on batteries. However, the limited lifespan of batteries restricts the size, power consumption, and applicability of these devices, requiring attention to battery replacement and maintenance. Sole reliance on battery power may not adequately support the growing complexity and scale of the IoT ecosystem.[6]

In recent years, there has been considerable interest in exploring energy harvesting solutions for the development of self-sustaining IoT devices.[7–10] Photovoltaic (PV) energy

R. Speranza, S. Amenta, P. Zaccagnini, C. F. Pirri, A. Lamberti
Department of Applied Science and Technology
Politecnico di Torino
Corso Duca Degli Abruzzi 24, 10129 Torino, Italy
E-mail: roberto.speranza@polito.it

The ORCID identification number(s) for the author(s) of this article can be found under https://doi.org/10.1002/aesr.202400370.

DOI: 10.1002/aesr.202400370

R. Speranza, P. Zaccagnini, C. F. Pirri, A. Lamberti
Center for Sustainable Future Technologies
Istituto Italiano di Tecnologia
10129 Torino, Italy

S. Amenta
Department of Science and Technological Innovation
Università degli Studi del Piemonte Orientale "Amedeo Avogadro"
Viale Teresa Michel 11, 15121 Alessandria, Italy

harvesting has emerged as a particularly promising opportunity in this field.[11–15] Within the context of indoor applications, several PV technologies stand out for their effectiveness in energy collection, including organic PVs, dye-sensitized solar cells (DSSCs), and perovskite solar cells. Each of these technologies offers unique characteristics that enable them to meet a variety of requirements across numerous applications.[16–19]

The growing interest regarding indoor photovoltaics (IPV) is reflected in the increased efforts from both academic and industrial players to develop more efficient, sustainable, and flexible IPV solutions.[20–29]

The sustainability of IPV, both in terms of the fabrication process and the materials used in the final device, has garnered significant interest. This is driven not only by the anticipated large-scale production of these products but also by their potential for direct contact and proximity to individuals in indoor environments.[30–33] While DSSCs are among the PV technologies that have reached commercialization, their relatively short energy payback time (EPBT) advantage primarily applies to outdoor applications.[6,34,35] For IPV, however, EPBT may not be one of the most relevant metrics, as these devices operate under low-light conditions and are designed to power low-power electronics, reducing battery waste rather than maximizing energy generation. Instead, sustainability assessments should consider factors such as material sustainability, lifecycle impact, and end-of-life management. Indeed, some of the few concerns about their safety and sustainability remain connected to the liquid electrolyte that is still needed for high efficiency solar cells.[36,37] Acetonitrile is usually used as a solvent for the preparation of the electrolyte, regardless of the chosen redox mediator. Unfortunately, acetonitrile is toxic and highly flammable and is characterized by high volatility.[38] For this reason, researchers have continuously looked for solutions to effectively avoid electrolyte leakage and evaporation.[39–43] On the other side, several efforts have been done to develop water-based DSSC, which would solve altogether the problem of using organic solvents for the electrolyte, with some optimization still needed to reach competitive values of conversion efficiency.[44–47]

Looking for a more sustainable alternative to organic solvents for the preparation of the electrolyte of electrochemical systems, recently Teoh and colleagues reported the possibility of using γ-valerolactone (γ-VL) as a sustainable and low-toxic solvent for supercapacitors.[48] γ-VL is a low-toxic solvent produced from cellulosic biomass, is biodegradable and presents low flammability, and being also less expensive than acetonitrile.[48–50] So far, this solvent has never been tested for the preparation of DSSC electrolyte. Therefore, in this work, γ-VL will be studied for DSSC fabrication and compared with acetonitrile (ACN) and 3-methoxypropionitrile (MPN), which are the most common solvents used for DSSC electrolyte preparations. It will be demonstrated that γ-VL is particularly well suited for the preparation of electrolytes for DSSCs intended for low-light conditions in indoor environments. Devices fabricated with this solvent exhibited an equal short circuit current, higher open circuit voltage, improved fill factor, and, consequently, enhanced efficiency compared to those prepared with ACN and MPN. Notably, these advantages were not observed under simulated solar light conditions.

2. Results and Discussion

2.1. Electrochemical Impedance Spectroscopy of Dummy Cells

To examine the impact of different solvents on the redox reaction at the DSSC counter electrode, electrochemical impedance spectroscopy (EIS) was conducted on symmetrical dummy cells. The results are displayed in **Figure 1**.

For each electrolyte formulation, the Nyquist plot revealed two primary semicircles. The one on the left-hand side corresponds to the iodide/triiodide redox reaction at the interface between the electrolyte and the Pt-coated electrodes. This is a fast process and is typically observed at frequencies around or above 1 kHz.[51–53] The low-frequency feature on the right is due to the mass transport diffusion of the reacting redox species from the surface of the Pt-coated counter electrode toward the bulk of the electrolyte.[54] Indeed, the consumption of reagents on the Pt-coated electrode, due to the redox reactions, results in an inhomogeneity of ion species concentrations within the electrolyte. The gradient will be equalized by ion diffusion. This process is slower than the redox reaction at the electrode surface and is observed at lower frequencies, below 10 Hz.[55] The separation of the two phenomena at the expected frequency can also be observed from the peak in the phase represented in Figure 1d.

In Figure 1e, it is reported the equivalent circuit used to model the system and fit the measured impedance spectra. The results of the fitting are reported as well in Figure 1. The circuit consists of a resistor R_s that models mainly the series resistance introduced by the FTO-coated electrode. The resistor R_{Pt} models the charge transfer resistance at the interface between the electrolyte and the electrode. At the same interphase, a constant phase element Q_{Pt} models the nonideal double layer capacitance, and a limited length Warburg element, Z_d, models the ion transport diffusion.[56]

$$Z_d = R_d \sqrt{\frac{\omega_d}{i\omega}} \tanh \sqrt{\frac{i\omega}{\omega_d}} \quad (1)$$

R_d is the diffusion resistance and ω_d is the characteristic frequency of the diffusion process.

On the Nyquist plot, R_{Pt} is approximately equal to the diameter of the high-frequency semicircle and gives information about the ease of the redox reaction. A smaller semicircle is generally observed for faster charge transfer. Therefore, based on the recorded spectra, it appears that this process was most effective in the ACN-based electrolyte, followed by the MPN-based electrolyte, and lastly, the γ-VL-based one. This evidence is confirmed also by the numerical values obtained for the circuit parameters reported in **Table 1**.

The values of the electrical parameters of the equivalent circuit have been reported as extracted from the Nyquist plot in Figure 1, but it must be underlined that the reported spectra were obtained from the EIS measurements performed on dummy cells. Therefore, assuming that the two counter electrodes to be identical, the values of R_{Pt} for a single electrode reported normalizing over the area would be 0.57, 7.0, and 17.1 $\Omega\,cm^2$ for ACN, MPN, and γ-VL cells, respectively. These values give a better estimation of the performance expected from the Pt-coated electrodes in combination with the studied electrolytes when employed in

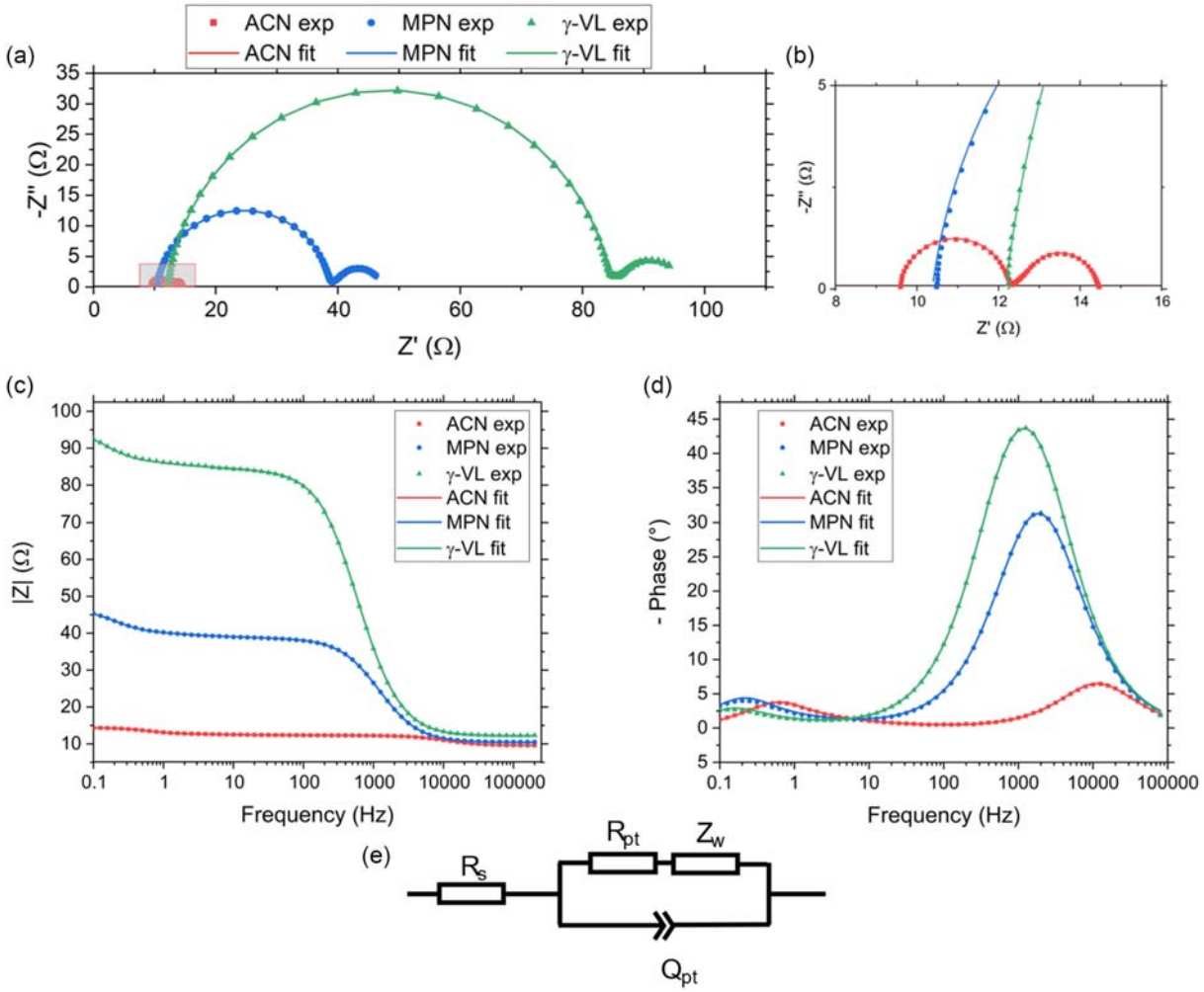

Figure 1. a) Comparison of EIS of dummy cells prepared with different electrolytes. b) Magnification of the impedance spectrum obtained for ACN electrolyte. Bode's plot representing c) impedance modulus and d) phase with respect to the frequency. e) Equivalent circuit used to fit the measured impedance spectra of the dummy cells. The experimental data (dots) and the results of the fitting (lines) are also reported.

Table 1. Parameters of the equivalent electrical circuit of the measured impedance spectra. The standard deviation values are calculated on the measurements performed on three identical devices for each electrolyte. The average X^2/|Z| was 0.00142, 0.00154, and 0.00314 for ACN, MPN, and γ-VL samples, respectively.

Electrolyte	R_{Pt} [Ω cm^2]	C_{Pt} [μF]	R_d [Ω]	ω_d [s^{-1}]	Solvent viscosity [mPa • s]	Electrolyte viscosity [mPa • s]
ACN	0.57 ± 0.09	8.9 ± 3.7	0.88 ± 0.28	1.6 ± 0.1	0.34[71]	0.57
MPN	7.0 ± 0.46	7.7 ± 3.2	3.7 ± 0.19	0.52 ± 0.03	1.1–1.6[71,72]	1.69
γ-VL	17.1 ± 1.2	6.9 ± 3.1	5.6 ± 0.4	0.38 ± 0.01	1.86–2.18[73,74]	2.88

the full DSSC. As a matter of fact, it was reported that, for good performing DSSC, R_{Pt} should have a value lower than 10 Ω cm^2.[51] Differently from the dummy cells with ACN and MPN, the one with γ-VL showed a R_{PGt} higher than this ideal value; therefore, it can be expected that some limitations in the DSSC performances could appear if γ-VL is exploited as solvent in the electrolyte, i.e., the reduction of I_3^- to I^- at the Pt counter electrode could be limited. Wettability studies were performed on the Pt-coated FTO-glass surface in combination with the prepared electrolyte to exclude any limitation coming from a

poor affinity between the solvents and the electrodes. The results are reported in Figure S1, Supporting Information. The measurements showed contact angles of 7.4°, 14.4°, and 10.4° for ACN, MPN, and γ-VL, respectively. These values indicate good wettability for all electrolytes, with ACN showing the most favorable case. MPN and γ-VL display similar values, with γ-VL exhibiting slightly better wettability on Pt-coated FTO glass. Based on these observations, it appears that electrode wettability is not a limiting factor in our devices and does not play a major role in the trends observed in our experimental results. The limitation in charge transfer resistance instead seems more related to the interaction between the solvent, the ions, and the surface of the electrode. One of the hypotheses to explain this behavior could be the higher tendency of γ-VL to coordinate I_2 molecules and thereby depleting the effective concentration of I_3^-, which could then be connected to the increased R_{Pt} observed from the measurements on γ-VL dummy cells. Indeed, Worsley et al. reported that this solvent exhibited a high ability to coordinate species showing Lewis's acidity, i.e., acting as electron pair acceptors. In their work the study focused on Pb^{2+} ions in perovskite crystal formation[57] On the other hand, differently from I^-, also I_2 and I_3^- can act as Lewis acids. To test this hypothesis, we performed UV–vis spectroscopy measurements in order to investigate the speciation within the I-based electrolytes, as previously reported in the literature.[58,59] Due to the high concentration of the electrolytes used in the electrochemical measurements, absorbance saturation was observed; therefore, the samples were diluted 1:4000 to obtain measurable spectra. However, for MPN, no useful spectrum could be recorded, as the intrinsic yellow color of the pure solvent masked the absorption peaks of the iodine-based species. The recorded absorbance spectra are reported in Figure S2, Supporting Information. UV–vis spectroscopy measurements showed that both can- and γ-VL based electrolytes display two characteristic absorption peaks at 290 and 360 nm, which have been attributed to I_3^-. Moreover, the absence of any peaks around 460 nm suggests that I_2 may not be present in measurable amounts.[58,59] Notably, while the peak positions remain consistent between the two solvents, the γ-VL system exhibits a significantly higher absorbance intensity. As a matter of fact, this observation may imply that γ-VL alters the coordination environment of I_3^- possibly increasing its molar absorptivity—without necessarily depleting its concentration via I_2 coordination, as our initial hypothesis had suggested. Such a modification in solvation might affect the redox behavior of I_3^-, potentially hindering its reduction kinetics at the Pt counter electrode. A deeper investigation into the mechanisms of solvent–ion interactions would be necessary to fully understand their behavior, but a detailed study is beyond the scope of this work, which is primarily aimed at elucidating the behavior of electrolytes within the operational context of solar cells. Nevertheless, these findings are still consistent with the increased R_{Pt} observed in the γ-VL dummy cells.

In addition to the differences observed in R_{Pt}, the fitted parameters also reveal clear trends in the R_d, which is associated with the mass transport of redox species within the electrolyte. As shown in Table 1, Rd increases notably from 0.88 Ω for ACN to 3.7 Ω for MPN and 5.6 Ω for γ-VL. This behavior correlates well with the measured viscosities of the electrolyte solutions, which progressively increase from 0.57 mPa s for ACN to 1.69 mPa s for MPN and 2.88 mPa s for γ-VL (Figure S3, Supporting Information). As expected, the addition of solutes to prepare the electrolytes results in increased viscosity with respect to literature values reported for pure solvents, but the relative order among ACN, MPN, and γ-VL is preserved. Higher viscosity affects ion mobility therefore limiting the diffusion of redox species such as I_3^- and I^- within the electrolyte. The observed increase in Rd then reflects this reduced diffusion efficiency. These findings are further supported by the decreasing values of ω_d, indicating a slower diffusion process in more viscous electrolytes. Therefore, both the redox reaction kinetics and the mass transport properties appear to be influenced by the physical properties of the solvents used in the electrolyte formulations and their interaction with the redox mediator.

2.2. Tafel Characterization of Dummy Cells

To further investigate the properties of the different electrolytes, Tafel measurements were performed on the dummy cells. The obtained Tafel plots are reported in **Figure 2**.

From a first qualitative analysis of the results, it is clear how the general behavior observed during EIS measurement is confirmed. Higher currents were generated by the ACN cell with respect to the MPN and γ-VL. As can be seen from **Table 2**, the ACN cell exhibited a limiting current of 46.4 mA cm^{-2}, much higher with respect to the ones recorded for MPN and γ-VL equal

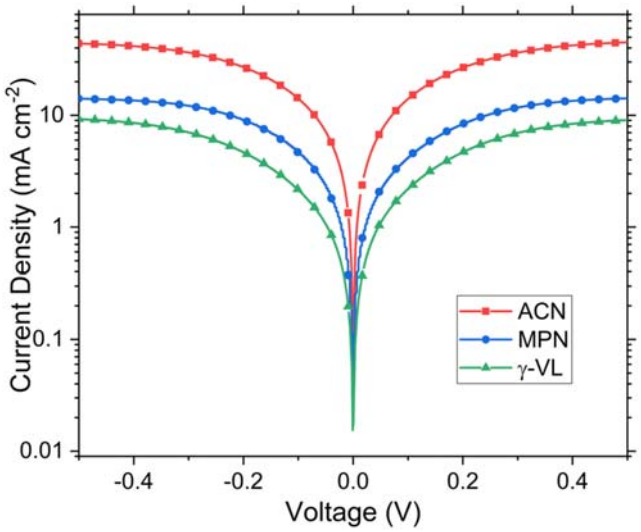

Figure 2. Tafel plot of dummy cells fabricated with different electrolytes formulation.

Table 2. Summary of the parameters extracted from the Tafel measurements on the dummy cells with different electrolytes. The standard deviation values are calculated on the measurements performed on three identical devices for each electrolyte.

Electrolyte	i_0 [mA cm^{-2}]	R_{Pt} [Ω cm^2]	i_{lim} [mA cm^{-2}]	D [cm^2 s^{-1}]
ACN	7.3 ± 0.1	1.7 ± 0.03	46.4 ± 2.8	(1.26 ± 0.08) × 10^{-5}
MPN	2.2 ± 0.2	5.8 ± 0.6	15.0 ± 0.8	(0.41 ± 0.02) × 10^{-5}
γ-VL	1.0 ± 0.2	13.1 ± 0.2	9.2 ± 0.7	(0.25 ± 0.02) × 10^{-5}

to 15.0 and 9.2 mA cm^{-2}. From these, the diffusion coefficients D of the I_3^- in the different electrolytes can be calculated.

$$D = \frac{d}{2nFC} J_{\text{lim}} \quad (2)$$

where d is the electrolyte thickness, C is the mediator concentration, n is the number of electrons involved in the reaction, here equal to 2, and F is Faraday's constant.[60]

Based on the results previously commented about the UV–vis spectroscopy measurement, for the calculation of the diffusion coefficient, the I_3^- concentration, which would be the limiting species affecting the limiting current in the Tafel measurements, was approximated with the concentration of I_2 in the electrolyte formulation, which is equal to 0.056 M. From the values reported in Table 2, the same trend is observed, with the values of D being in line with the values reported in the literature.[55] Moreover, MPN and γ-VL reach their limiting current for voltage values much lower than ACN. From this point of view, it is interesting to see that for MPN, a plateau in the current is observed for lower voltage values than γ-VL. This could be explained by the fact that, in both cases, the higher viscosity can cause mass transport limitation in the current. In spite of that, by using MPN, the redox reaction at the electrodes is facilitated, enabling the current to increase quicker as higher (absolute) voltage is applied to the cell. This is in line with the observations made during the EIS measurements regarding the R_{Pt} obtained with the three electrolytes.

To further investigate this aspect, the measurements were analyzed according to the differential Tafel plot approach, to find the exchange current values i_0 for the three electrolytes.[61,62] i_0 can be related to the charge transfer resistance R_{Pt} at the electrode–electrolyte interface by

$$i_0 = \frac{RT}{nFR_{\text{Pt}}} \quad (3)$$

where R is the gas constant, T is the temperature, n is the number of electrons involved in the reaction, here equal to 2, and F is Faraday's constant.[60] The results are reported in Table 2.

The values of i_0 and the corresponding results obtained for R_{pt} confirm the same observations made during the EIS measurements. Indeed, γ-VL leads to the lowest exchange current, and therefore, the highest R_{pt}, with respect to MPN and ACN. Moreover, the values of R_{pt} extracted from the Tafel measurements are quite consistent with the results obtained from the EIS measurements.

The role of redox species diffusion in the γ-VL-based electrolyte was analyzed with additional Tafel measurements performed on dummy cells with varying spacer thicknesses. The results are reported in Figure S4, Supporting Information. As anticipated, an increase in the inter-electrode distance led to a marked decrease in the limiting current, confirming that mass transport limitations are more pronounced in the γ-VL system. These observations clearly suggest how reducing the distance between the electrodes would represent a viable route for performance optimization. Finally, to explore potential strategies to achieve a balance between efficiency and sustainability, we also repeated the Tafel measurements with an electrolyte composed of a 1:1 v/v mixture of ACN and γ-VL. The results are also reported in Figure S4, Supporting Information. This mixed-solvent formulation exhibited both higher exchange and limiting currents compared to pure γ-VL, indicating improved ion mobility and reduced diffusion resistance, showing how blending γ-VL with a lower-viscosity solvent such as ACN could offer a viable route to balancing device performance with the use of more environmentally benign components. While a systematic study of mixed-solvent electrolytes lies beyond the scope of the present work, we consider this a promising direction for future research in the development of sustainable DSSC systems.

2.3. Current–Voltage Characterization of DSSCs

Once the overall behavior of the electrolytes was evaluated in dummy cells, the same formulations were tested in full DSSC configuration. The devices were tested first under standard AM1.5 G illumination conditions at 1 sun, and the results are reported in **Figure 3** and **Table 3**.

The J–V measurements performed under 1 sun light intensity showed unsurprisingly that the ACN DSSC was the best performing one, with an average conversion efficiency of 6.25 %, which is in line with the results reported for lab cells fabricated with the same materials.[63] The highest efficiency was enabled

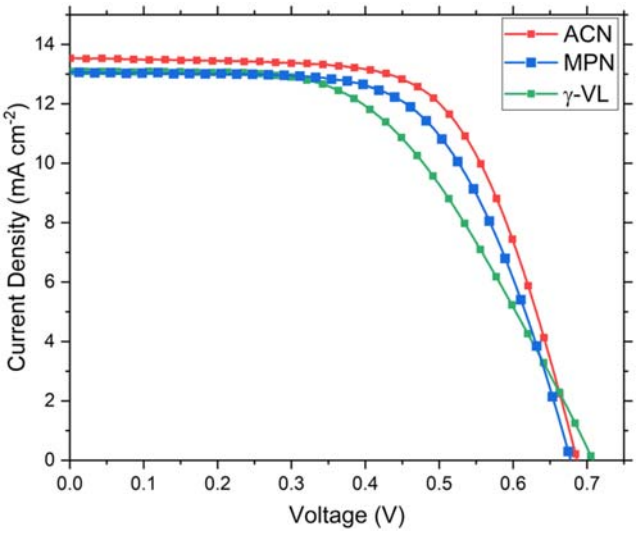

Figure 3. J–V characteristic of DSSCs fabricated with different electrolyte formulations under AM1.5 G conditions at 1 sun.

Table 3. Photovoltaic parameters of DSSCs with different electrolyte formulations tested under AM1.5G conditions. The average and standard deviation values are calculated on the measurements performed on three identical devices for each electrolyte.

Electrolyte	J_{sc} [mA cm^{-2}]	V_{oc} [V]	FF	η [%]
ACN	13.4 ± 0.4	0.69 ± 0.01	0.67 ± 0.02	6.25 ± 0.28
MPN	13.2 ± 0.2	0.68 ± 0.01	0.59 ± 0.04	5.25 ± 0.30
γ-VL	13.2 ± 0.3	0.70 ± 0.01	0.54 ± 0.01	4.93 ± 0.22

especially by the highest fill factor achieved by the ACN cell with respect to the other two. This difference is not surprising considering the properties of the different electrolytes, as discussed in the previous section regarding the measurements performed on dummy cells. The less viscous ACN allowed better ionic transport and seem to have a lower impact on the overall series resistance of the DSSC, by that means improving the FF. This is also observed in the *J–V* curve where, for voltage values close to the V_{oc}, the current in the ACN cell exhibits a more vertical behavior, differently from the case of MPN and γ-VL that shows a lower slope, which is a known effect of a higher series resistance in the cell.[64] Here also the lower R_{Pt} observed for ACN in the dummy cell's measurements might contribute to the higher *FF*. The opposite consideration can be done for γ-VL, which had the lowest average *FF* of 0.54. This parameter is definitely limited by the higher viscosity as well as the nonoptimal combination with the Pt counter electrode in terms of exchange current and charge transfer resistance (Table 2). Notably, the short circuit current (J_{sc}) density obtained for γ-VL, equal to 13.2 mA cm^{-2}, reached a slightly higher value with respect to the J_{lim} recorded in the Tafel plot measurements performed on the dummy cells with the same electrolyte. This results can be reasonably attributed to slight variations in electrolyte layer thickness inherent to the two device configurations. Although both setups were sealed using the same thermoplastic spacer, the effective distance between electrodes differs due to the structural composition of the cells. In DSSCs, the presence of the mesoporous TiO_2 photoanode reduces the actual spacing between the Pt-coated counter electrode—where triiodide reduction occurs—and the dye-sensitized surface of the photoanode—where iodide oxidation takes place. Moreover, under illumination, the fast dye regeneration at the photoanode establishes a steeper concentration gradient compared to dummy cells. This gradient can enhance triiodide diffusion toward the counter electrode resulting in a higher short circuit current density than the limiting current observed in dummy cells, as it was also reported in the literature.[65] These results align well also with the measurements done on dummy cells with reduced spacer thickness reported in Figure S4, Supporting Information and previously commented.

One last observation could be made regarding these measurements regarding the V_{oc} obtained with different electrolytes, with the one reported for γ-VL slightly higher than the other two. This might be connected again to the higher ability of γ-VL to coordinate I_3^- ions discussed in the previous section. Here this effect could be

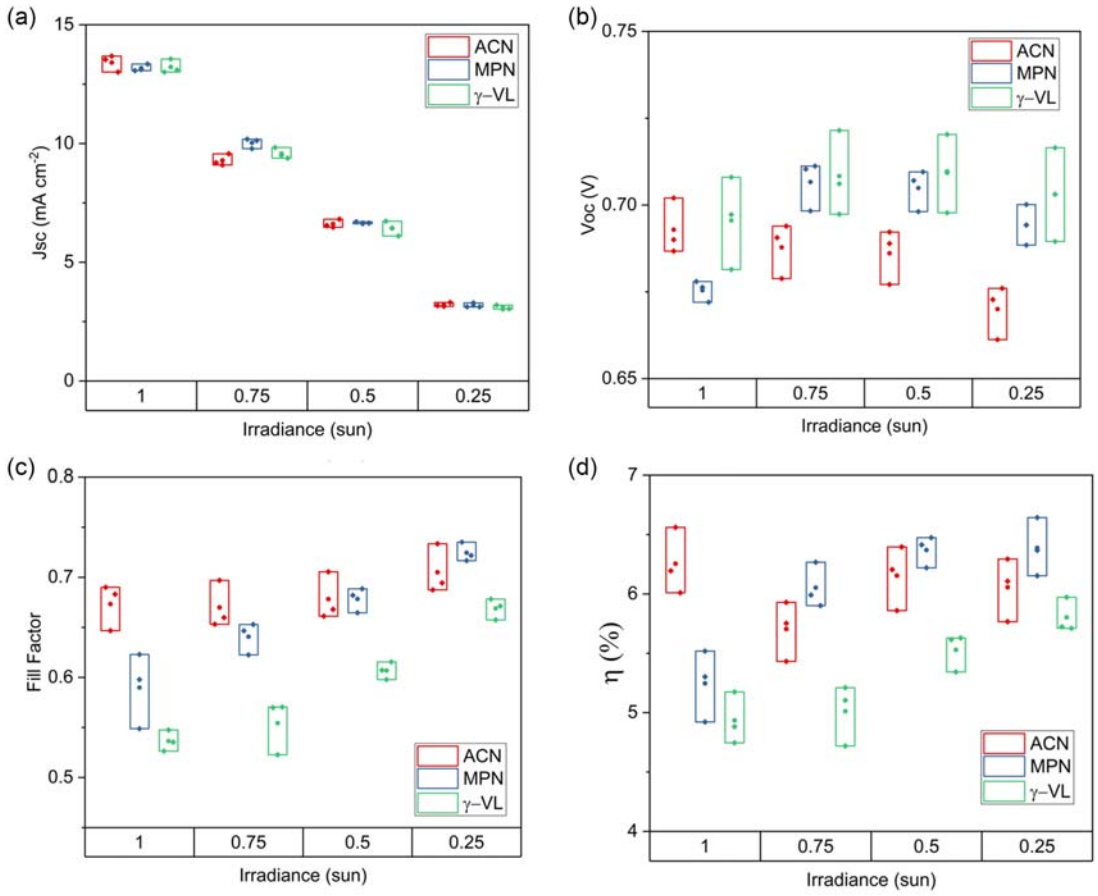

Figure 4. Comparison of photovoltaic parameters obtained at different irradiance level under AM1.5 spectrum for DSSCs fabricated with different electrolyte formulations. In a) the short circuit current, in b) the open circuit voltage, in c) the fill factor and in d) the rated efficiences. The box charts report the data for three devices for each electrolyte and the relative average value.

beneficial from the point of view of reducing parasitic recombination at the TiO_2–electrolyte interface, thereby increasing the V_{oc}.[66]

In order to investigate the performance of the solvents in cells working at low-light illumination condition, *J–V* measurements were repeated under reduced simulated AM1.5 G light intensity to 0.75, 0.5, and 0.25 sun. Moreover, the DSSCs were also tested under indoor illumination, using an LED warm light with illuminance values of 1000 lux, 500 lux, and 100 lux, which corresponded to an irradiance of 330, 167, and 39 μW cm^{-2}. The results are reported in **Figure 4** and **5**. From the comparison of the PV parameters under different illumination conditions, it is clear how even at reduced light intensities, under simulated solar illumination the DSSC based on γ-VL resulted to be the least performing one, presumably for the same reasons previously discussed for the 1 sun light intensity.

On the other hand, looking at the results obtained under indoor illumination conditions reported in Figure 5, a complete turnaround is observed. When characterized under LED indoor illumination up to 100 lux illuminance, corresponding to an extremely low irradiance of 39 μW cm^{-2}, γ-VL achieved the highest conversion efficiency of 14.9%, compared with the values obtained for ACN and MPN equal to 8.8 and 12.3%, respectively. As it can be seen from the PV parameters reported in **Table 4**, this result is mainly related to the higher J_{sc} and V_{oc} obtained with the γ-VL cell with respect to the other two.

Looking at the indoor *J–V* curves reported in **Figure 6**, it can be seen that in this case the different viscosity does not have an impact on the series resistance of the DSSC, as the slope of the *J–V* curve at high voltage values is the same for the three cells. Instead, the reduction in the FF of the ACN cell is clearly related to the steeper slope of the curve voltages close to 0 V. This feature is described by a lower shunt resistance in the DSSC, which usually comes from higher parasitic electron recombination at the photoanode.[67]

Finally, most of all the higher conversion efficiency comes from the higher V_{oc} and the higher J_{sc} achieved by γ-VL with respect to ACN and MPN. The reason for this has been already

Table 4. Photovoltaic parameter of DSSC with different electrolyte formulation tested under LED warm light illumination at 100 lux (39 μW cm^{-2}).

Electrolyte	J_{sc} [μA cm^{-2}]	V_{oc} [V]	FF	η [%]
ACN	15.5 ± 0.4	0.41 ± 0.01	0.55 ± 0.02	8.8 ± 0.4
MPN	15.6 ± 2.1	0.49 ± 0.01	0.63 ± 0.04	12.3 ± 1.4
γ-VL	17.6 ± 0.3	0.52 ± 0.02	0.64 ± 0.01	14.92 ± 0.6

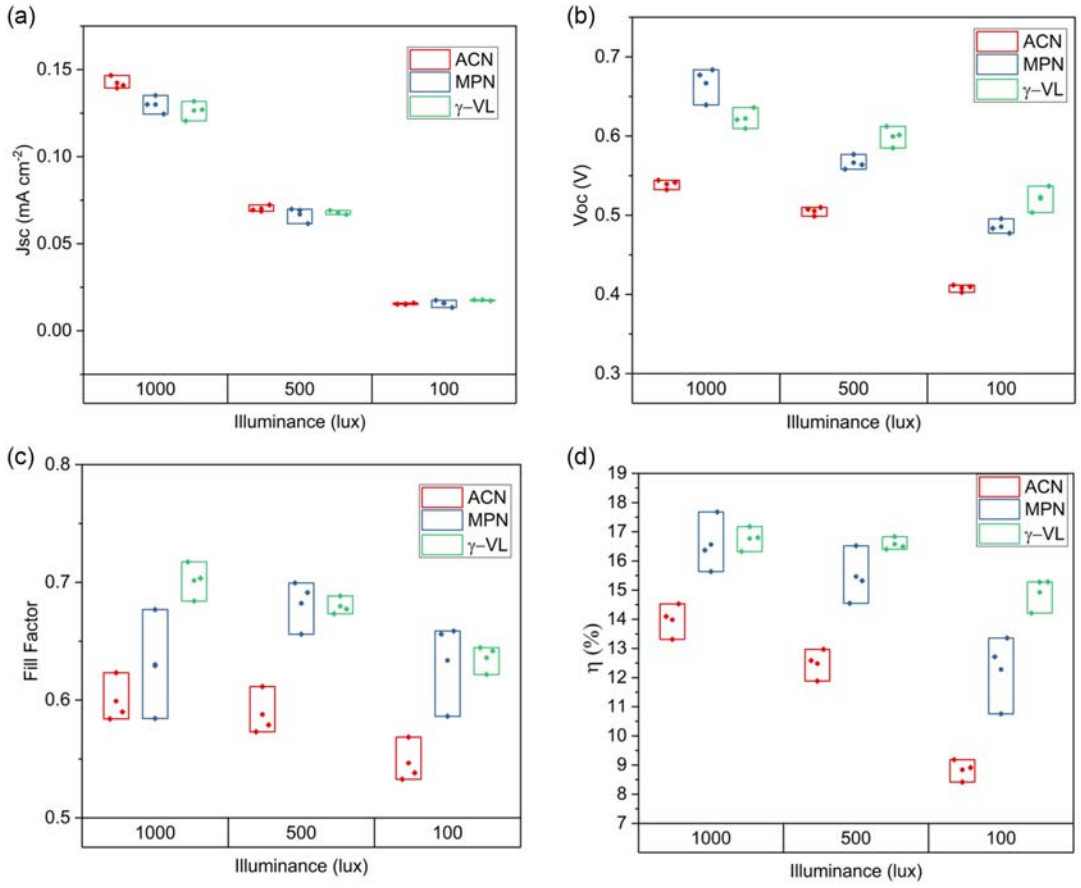

Figure 5. Comparison of photovoltaic parameters obtained at different illuminance level under LED indoor condition for DSSCs fabricated with different electrolyte formulations. In a) the short circuit current, in b) the open circuit voltage, in c) the fill factor and in d) the rated efficiences. The box charts report the data for three devices for each electrolyte and the relative average value.

discussed in relation to simulated solar illumination, but it is clear how this property becomes crucial and clearly noticeable under indoor illumination conditions.

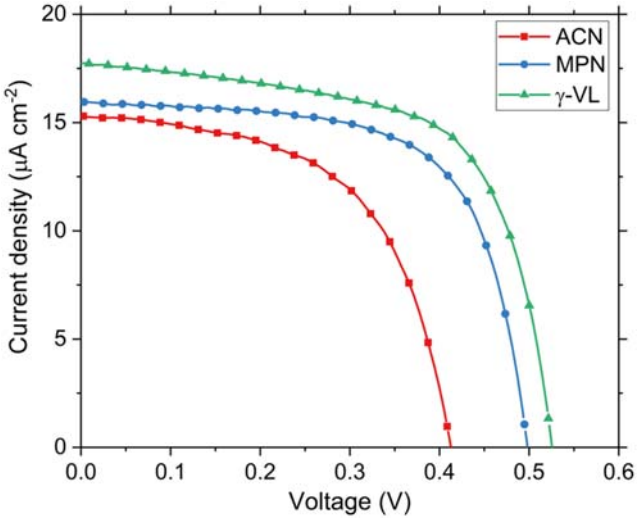

Figure 6. *J–V* characteristics recorded under warm white LED indoor light illumination at 100 lux (39 μW cm^{-2}) of DSSC fabricated with different electrolyte formulations.

2.4. Electrochemical Impedance Spectroscopy of Dye-Sensitized Solar Cells

EIS measurements were performed on the DSSC as well, under dark conditions and with an applied voltage bias of 0.7 V, equal to the V_{oc} shown by the DSSCs. These conditions were selected in order to investigate the electron recombination at the photoanode, which seemed to be the crucial factor determining the performance difference between the DSSC fabricated with different solvents. The results of the EIS measurements and the circuit used to fit the impedance spectra are reported in **Figure 7**. Indeed, under dark conditions, for high-voltage bias, the TiO_2 in the photoanode enter in its conductive state, meaning that the electron transport resistance within the semiconductor R_t is much lower than the charge transfer resistance R_r at the TiO_2–electrolyte interface. In this condition, R_r can be estimated by the EIS measurements, fitting the Nyquist plot. The values of the electrical parameters extracted from the fitting are reported in **Table 5**.[53]

The EIS measurements confirm the observation done previously regarding the impact of different solvents in the electrolyte on the DSSC performances. Indeed, the same trend observed for the dummy cell measurement regarding the charge transfer resistance at the counter electrode R_{pt} can be found here. Although a higher value than expected was measured for the ACN case, nonetheless, is still considered acceptable for good DSSC operation.

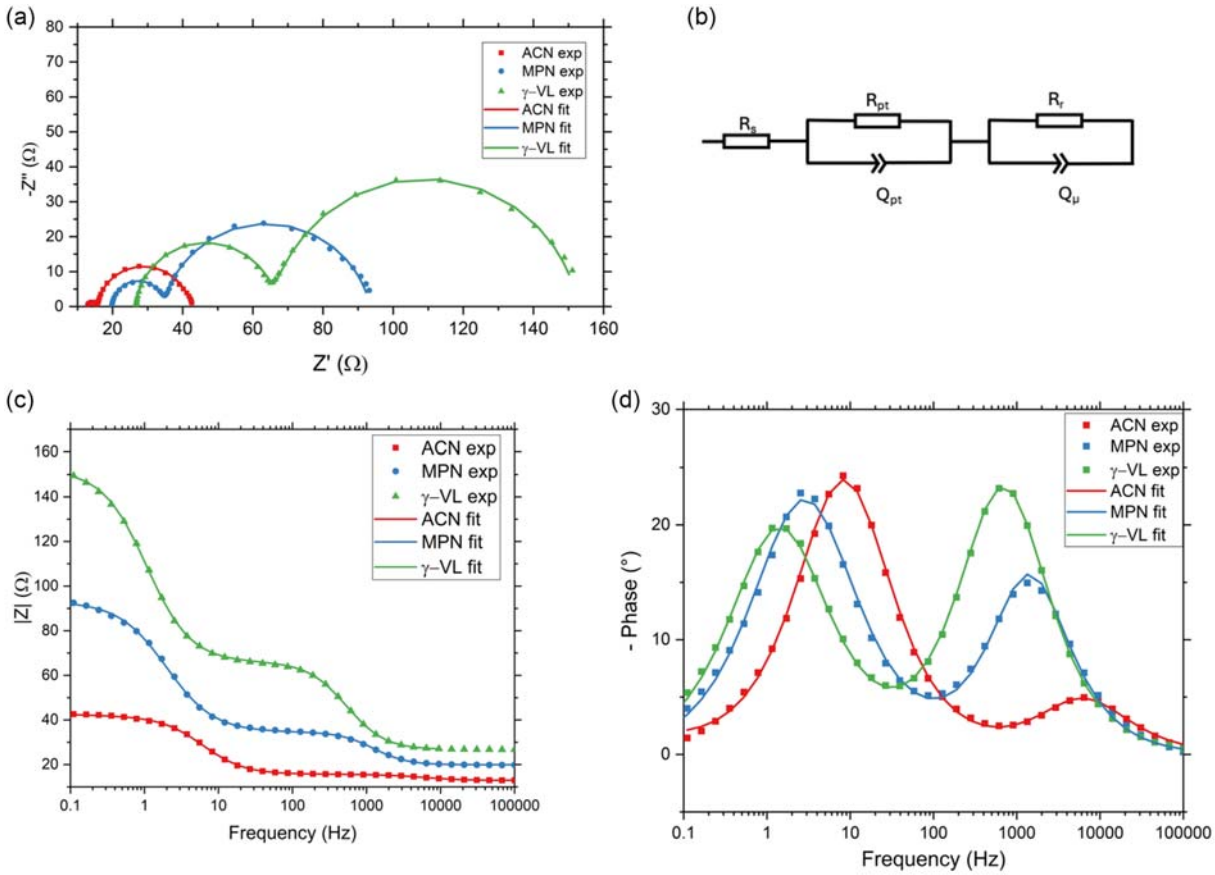

Figure 7. a) Nyquist plot of DSSC fabricated with different electrolytes recorded at 0.7 V applied bias under dark conditions and b) equivalent circuit used to fit the measured impedance spectra. Bode's plot representing impedance modulus c) and phase d) with respect to the frequency.

The main differences here were found regarding the electrical parameters modeling the photoanode–electrolyte interfaces, i.e., the recombination resistance R_r and the chemical capacitance C_μ, which is related to the change of electron density within the TiO_2.[53]

Notably, γ-VL caused the highest recombination resistance with respect to the other cells, while ACN was the one with the lowest R_r. This evidence gives further confirmation of the ability of γ-VL to reduce the unwanted electron recombination with the I_3^- ions at the interface with the TiO_2. The main two reasons that could explain this phenomenon could be related to already mentioned peculiar interaction of the γ-VL with the I_3^- ions and to the possible tendency of γ-VL to adsorb on the free space on the TiO_2 photoanode due to its Lewis basicity, suppressing the back electron transfer to I_3^- as it happens also with in a manner similar to pyridine-based additives like TBP.[66,68,69] The higher adsorption of γ-VL onto the TiO_2 might be supported also by the higher C_μ showed by the γ-VL with respect to the other solvents. Indeed, the chemical capacitance is proportional to the density of electrons in the semiconductor conduction band.[53] To further investigate how the different solvents affect the DSSC behavior under working conditions, in combination with photo-activated processes, the EIS measurement at V_{oc} were repeated under constant illumination of 0.1 sun. In these conditions, the dye injects electron into the TiO_2 conduction band, therefore increasing the charge carrier density within the semiconductor. The results are reported in Figure S5, Supporting Information, and the parameter extracted from the fit of the impedance spectra are reported in Table S1, Supporting Information. As expected, under illumination conditions, the charge transfer reaction at the counter electrode appears almost unaffected, with the same trend observed also under dark conditions. At the photoanode instead, some differences were observed. Indeed, γ-VL showed average values of R_r and C_μ of 71.1 Ω and 3.3 mF. As expected, these values were reduced with respect to the values observed in dark,

Table 5. Parameters of the equivalent electrical circuit of the measured impedance spectra. The standard deviation values are calculated on the measurements performed on three identical devices for each electrolyte. The average X^2/|Z| was 0.0022, 0.0032, and 0.0042 for ACN, MPN, and γ-VL samples, respectively.

Electrolyte	R_{Pt} [Ω cm^{-2}]	C_{pt} [μF]	R_r [Ω]	C_μ [mF]
ACN	1.2 ± 0.3	14.1 ± 8.3	35.3 ± 12.3	2.1 ± 0.6
MPN	4.8 ± 0.7	21.8 ± 1.8	61.6 ± 4.2	3.2 ± 0.4
γ-VL	15.1 ± 3.9	16.3 ± 2.9	89.7 ± 23.2	4.2 ± 0.75

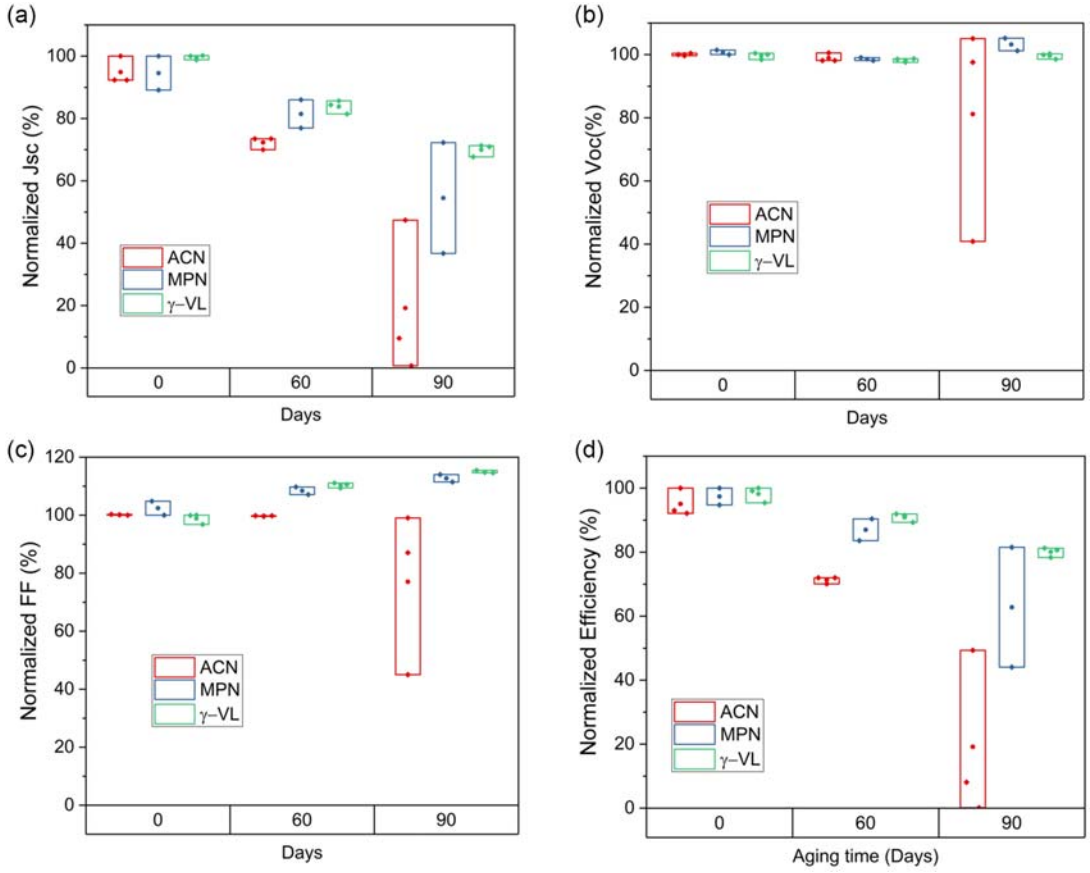

Figure 8. Aging of normalized photovoltaic parameters of DSSCs fabricated with different solvents kept in the dark at room temperature. In a) the short circuit current, in b) the open circuit voltage, in c) the fill factor and in d) the rated efficiences. The box charts report the data for three devices for each electrolyte and the relative average value.

which has been connected to the higher concentration of I_3^- close to the TiO_2 particles due to the dye regeneration and to the electron injection inside the semiconductor.[53] If compared with the results observed for ACN and MPN, γ-VL still appear to allow a reduction of injected photoelectron recombination with triiodide ions. Indeed, if the rate constant for recombination is calculated from $\omega_r = 1/(R_r C_\mu)$, average values of 4.28, 7.16, and 30.3 s^{-1} are obtained for γ-VL, MPN, and ACN, respectively, showing the same trend in recombination reactions observed for the measurements in dark.

2.5. Long-Term Stability

To evaluate how the different solvents in the electrolyte could impact the long-term stability of the DSSC, the performances of the fabricated cells were tested after two and three months of storage in the dark at room temperature according to ISOS-D1 protocol.[70] The results are reported in **Figure 8**. As it can be seen from the variation of the normalized PV parameters, γ-VL and MPN had almost identical behavior. After two months, both of them retained a conversion efficiency close to 90% of their initial value. Instead, for ACN, efficiency dropped to 70% of the initial value. After three months of storage in the dark, the device prepared with γ-VL showed overall the best stability retaining 80% of their initial efficiency. This behavior is mainly related to the slow electrolyte evaporation that can be identified, mainly, in the reduction of the photogenerated current, as it can be seen from Figure 8a. Indeed, the FF and the Voc remained almost unchanged for all the tested cells.

It is clear then how the higher volatility of ACN with respect to the other two solvents can introduce limitations from the point of view of long-term stability, even in indoor environment where the operation conditions are not as stressful for solar cells as it is in outdoor conditions, where intense sunlight can cause strong temperature variations in the cells, accelerating their degradation.

3. Conclusion

In this work, it was investigated the possibility of using γ-valerolactone as a green and low-toxic solvent in the electrolyte preparation for DSSCs. Three different iodine-based electrolytes were fabricated, changing the solvents and keeping all the other parameters constant. The compared solvents were acetonitrile (ACN), 3-methoxypropionitrile (MPN), and γ-valerolactone (γ-VL). First, the three electrolytes were tested in symmetrical dummy cells by EIS measurements and Tafel polarization measurements. It was observed that γ-VL behavior was very similar to the one of MPN, mostly because of their viscosity much higher than ACN. MPN and γ-VL showed mass transport limitations that instead were absent in ACN. Moreover, γ-VL exhibited a higher charge transfer resistance at the counter electrode with respect to MPN. From these observations, it might seem that γ-VL would not be suitable as a solvent for electrolyte preparation in DSSC operated under strong light intensity conditions, such as outdoor operation under sunlight illumination. This conclusion is confirmed by the current–voltage measurements performed on full DSSC device fabricated using the three different electrolytes. Under AM1.5 G simulated solar illumination, the cell fabricated with γ-VL showed the lowest overall performances in terms of conversion efficiency, mainly fill factor with respect to the other two solvents. These results are in good agreement with the ones obtained from the dummy cells measurements and further confirm the limitation that γ-VL could introduce in standard operating conditions.

Nevertheless, completely different and surprising results were obtained under indoor illumination conditions. When the DSSC were tested under the illumination provided by a warm white LED light set to three different illuminance levels (1000, 500, and 100 lux), γ-VL provided the best performances among the fabricated cells. When the light intensity is strongly reduced, the higher viscosity of γ-VL and the higher charge transfer resistance previously observed did not have a detrimental impact on the solar cell performances. Instead, γ-VL has beneficial effect on the open-circuit voltage generated by the DSSC under indoor condition, thanks to a reduction of the electron recombination at the photoanode and a possible negative shift its conduction band level. These observations were confirmed by EIS measurements performed on the fabricated cells. Moreover, long-term stability tests indicated that γ-VL provided the same behavior of MPN under prolonged storage in indoor conditions, outperforming the more volatile ACN.

In conclusion, the results reported in this work suggested that γ-VL can represent a good sustainable and safe alternative to more toxic solvents such as ACN and MPN for indoor DSSCs.

4. Experimental Details

Materials: Fluorine-doped tin oxide (FTO)-coated glass (7 Ω sq^{-1}), thermoplastic sealing film (60 μm, Meltonix), Amosil 4 two component glue, Ruthenizer 535-bisTBA (N719, dye), transparent TiO_2 nanoparticles paste (Ti-Nanoxide T/SP), reflective TiO_2 nanoparticle paste (Ti-Nanoxide R/SP), and Ti-Nanoxide BL/SC were purchased from Solaronix. Sodium iodide (NaI), iodine (I_2), and γ-valerolactone were purchased from Sigma-Aldrich, while MPN, acetonitrile, and 4-*tert*-butylpyridine (TBP) were purchased from Merck.

DSSC and Symmetrical Dummy Cell Fabrication: FTO-coated glasses were cleaned in an ultrasonic bath for 30 min in a solution of deionized water and detergent, acetone and ethanol, successively. Then, they were put on a hot plate for 10 min at 100 °C to ensure complete solvent evaporation. Photoanodes preparation was carried out by depositing a thin layer of Ti-Nanoxide BL/SC via spin coating (5000 rpm for 30 s, acceleration 2000 rpm s^{-1}) which was then fired at 500 °C for 40 min to obtain a compact TiO_2 blocking layer. Then three layers of transparent TiO_2 paste and one layer of reflective TiO_2 paste were printed on the blocking layer-coated FTO glasses by screen printing technique (61–64 mesh). Each layer was dried for 10 min at 100 °C to evaporate the solvent. Then, the photoanodes were fired to ensure the complete removal of solvent and additive residuals and to interconnect the TiO_2 particles for better charge collection. The samples were heated from room temperature to 475 °C with a ramp of 120 °C h^{-1}. Then they were kept at 475 °C for 30 min, and then they were cooled down to 70 °C in 5 h. The area of the deposited photoanodes was 0.36 cm^2, while their thickness was measured to be between 13 ± 1 μm. Right after the calcination, the photoanodes were soaked in dye

solution for 18 h to ensure complete sensitization. The sensitizing solution was prepared dissolving 0.3 mM of N719 in ethanol. Counter electrodes were fabricated by coating the FTO glasses with a thin layer of Pt by sputtering technique. The deposition was carried out with a Q150T ES sample preparation system (Quorum Technologies Ltd). The different electrolytes were tested with the following composition: 0.45 M NaI, 0.056 M I_2, and 0.55 M 4-*tert*-butylpyridine dissolved either in ACN, MPN, or γ-VL, respectively. The devices were sealed by means of the Meltonix film and the Amosil 4 two component glue was used as an additional sealing. For each electrolyte, three DSSCs were fabricated to study reproducibility.

The fabrication of symmetrical dummy cell was performed by assembling two identical Pt-coated counter electrodes, sealed with a film of Meltonix, and filled with the different electrolyte formulations. For the measurements performed at different spacer thickness, one, two, and three Meltonix layers were used to seal the cell and additional pressure was applied to further reduce the thickness of the thermoplastic during melting. The resulting spacer thickness was measured from the overall device thickness, subtracting the glass electrode thickness.

Characterization: EIS measurements and linear polarization measurements were performed with a Autolab PGSTAT128 potentiostat equipped with an FRA32M module. EIS measurements were performed in the frequency range between 100 kHz and 100 mHz, with a small signal amplitude of 10 mV. The scan speed for the Tafel measurement was 10 mV s^{-1}. The same instrument was used to collect the current density–voltage (*J*–*V*) response of the DSSC. The *J*–*V* curves were recorded with a scan rate of 20 mV s^{-1}. A Newport 91195 A solar simulator was used to perform the measurements under AM 1.5 G light spectrum, while a warm white LED lamp (12–60 V AC/DC, 10 W, 3000 K, 810 lm from SPL) was used for the measurement under indoor illumination conditions and measured with a Delta Ohm HD 2102.2 photo/radiometer. Rheological measurements were performed by means of Antoon Paar MCR302 rheometer. The measurement was performed with a parallel plate system of 25 mm diameter with a sample measurement thickness of 0.2 mm. The measurements were performed at 25 °C in a shear rate range of [1000:10 000] 1/s compatible for all the tested samples. The interval was sampled 11 points per decade. Contact angle measurements were performed with a Contact Angle System OCAH 200 by Dataphysics. UV–vis measurements were performed with a U-5100 UV-Vis Spectrometer from Hitachi.

Supporting Information

Supporting Information is available from the Wiley Online Library or from the author.

Acknowledgements

This work was partially funded by the project "nuovi Concetti, mAteriali e tecnologie per l'iNtegrazione del fotoVoltAico negli edifici e in uno scenario di generazione diffuSa" ("CANVAS"), funded by the Italian Ministry of the Environment and the Energy Security, through the Research Fund for the Italian Electrical System (type-A call, published on G.U.R.I. n. 192 on 18-08-2022). This work was conducted within the Technologies for Sustainability Flagship of the Istituto Italiano di Tecnologia. This article was partially funded under the National Recovery and Resilience Plan (NRRP), Mission 4 "Education and Research"—Component 2 "From research to business"—Investment 3.1 "Fund for the realization of an integrated system of research and innovation infrastructures"—Call for tender No. n. 3264 of 28/12/2021 of Italian Ministry of Research funded by the European Union—NextGenerationEU—Project code: IR0000027, Concession Decree No. 128 of 21/06/2022 adopted by the Italian Ministry of Research, CUP: B33C22000710006, Project title: iENTRANCE. Also, this study was carried out within the MOST—Sustainable Mobility Center and received funding from the European Union Next-GenerationEU (PIANO NAZIONALE DI RIPRESA E RESILIENZA (PNRR)—MISSIONE 4 COMPONENTE 2, INVESTIMENTO 1.4—D.D. 1033 17/06/2022, CN00000023). This manuscript reflects only the authors' views and opinions, neither the European Union nor the European Commission can be considered responsible for them.

Conflict of Interest

The authors declare no conflict of interest.

Data Availability Statement

The data that support the findings of this study are available from the corresponding author upon reasonable request.

Keywords

γ-valerolactone, dye-sensitized solar cells, electrolytes, indoor photovoltaics, recombination, solvent, sustainability

Received: October 31, 2024
Revised: May 31, 2025
Published online: July 24, 2025

[1] J. Davies, C. Fortuna, *The Internet of Things: From Data to Insight* (Eds: J. Davies, C. Fortuna), John Wiley & Sons, Inc, Hoboken, NJ **2020**.
[2] Q. F. Hassan, *Internet of Things A to Z: Technologies and Applications*, John Wiley, Hoboken **2018**.
[3] V. Tsiatsis, S. Karnouskos, J. Höller, D. Boyle, C. Mulligan, *Internet of Things: Technologies and Applications for a New Age of Intelligence*, 2nd edition, Academic Press, London San Diego, CA Cambridge, MA Oxford **2019**.
[4] D. Minoli, K. Sohraby, B. Occhiogrosso, *IEEE Internet Things J.* **2017**, *4*, 269.
[5] V. Moudgil, K. Hewage, S. A. Hussain, R. Sadiq, *Renew. Sustain. Energy Rev.* **2023**, *174*, 113121.
[6] V. Pecunia, L. G. Occhipinti, R. L. Z. Hoye, *Adv. Energy Mater.* **2021**, *11*, 2100698.
[7] N. Pataki, P. Rossi, M. Caironi, *Appl. Phys. Lett.* **2022**, *121*, 230501.
[8] S. Naifar, O. Kanoun, C. Trigona, *Sensors* **2024**, *24*, 4688.
[9] G. Clementi, I. Neri, F. Cottone, A. Di Michele, M. Mattarelli, L. Sforna, S. Chiappalupi, G. Sorci, A. Michelucci, L. Catacuzzeno, L. Gammaitoni, *Nano Energy* **2024**, *121*, 109211.
[10] R. De Fazio, D. Cafagna, G. Marcuccio, A. Minerba, P. Visconti, *Energies* **2020**, *13*, 2161.
[11] A. Chakraborty, G. Lucarelli, J. Xu, Z. Skafi, S. Castro-Hermosa, A. B. Kaveramma, R. G. Balakrishna, T. M. Brown, *Nano Energy* **2024**, *128*, 109932.
[12] D. Müller, E. Jiang, P. Rivas-Lazaro, C. Baretzky, G. Loukeris, S. Bogati, S. Paetel, S. J. C. Irvine, O. Oklobia, S. Jones, D. Lamb, A. Richter, G. Siefer, D. Lackner, H. Helmers, C. Teixeira,

D. Forgács, M. Freitag, D. Bradford, Z. Shen, B. Zimmermann, U. WürfelACS Appl. Energy Mater. **2023**, *6*, 10404.
[13] J. Barichello, P. Mariani, L. Vesce, D. Spadaro, I. Citro, F. Matteocci, A. Bartolotta, A. Di Carlo, G. Calogero, *J. Mater. Chem. C* **2024**, *12*, 2317.
[14] K. Seunarine, Z. Haymoor, M. Spence, G. Burwell, A. Kay, P. Meredith, A. Armin, M. Carnie, *J. Phys. Energy* **2024**, *6*, 015018.
[15] R. Speranza, P. Zaccagnini, A. Sacco, A. Lamberti, *Solar RRL* **2022**, *6*, 2200245.
[16] L. Mauri, A. Colombo, C. Dragonetti, F. Fagnani, *Inorganics* **2022**, *10*, 137.
[17] F. Grifoni, M. Bonomo, W. Naim, N. Barbero, T. Alnasser, I. Dzeba, M. Giordano, A. Tsaturyan, M. Urbani, T. Torres, C. Barolo, F. Sauvage, *Adv. Energy Mater.* **2021**, *11*, 2101598.
[18] L. Vesce, P. Mariani, M. Calamante, A. Dessì, A. Mordini, L. Zani, A. Di Carlo, *Solar RRL* **2022**, *6*, 2200403.
[19] *Organic and Printed Electronics: Fundamentals and Applications*, 2nd Edition (Eds: G. Nisato, D. Lupo, S. Rudolf), Jenny Stanford Publishing, Singapore **2024**.
[20] "LAYER, a technology that harvests energy from ambient light, even in extremely low-light conditions," https://dracula-technologies.com/technology-layer/ (accessed: October, 2024).
[21] "Powerfoyle Patented Solar Cell Technology," https://www.exeger.com/powerfoyle/ (accessed: October, 2024).
[22] "Powering tomorrow. Organically. Epishine Explained," https://www.epishine.com/epishine-explained (accessed: October, 2024).
[23] Z. Shen, F. T. Eickemeyer, J. Gao, L. Pfeifer, D. Bradford, M. Freitag, S. M. Zakeeruddin, M. Grätzel, *Chem* **2023**, *9*, 3637.
[24] G. Gianola, R. Speranza, F. Bella, A. Lamberti, *Sol. Energy* **2023**, *265*, 112116.
[25] Z. Skafi, J. Xu, V. Mottaghitalab, L. Mivehi, B. Taheri, F. Jafarzadeh, S. K. Podapangi, D. Altamura, M. R. Guascito, L. Barba, C. Giannini, A. Rizzo, F. De Rossi, H. Javanbakht Lomeri, L. Sorbello, F. Matteocci, F. Brunetti, T. M. Brown, *Solar RRL* **2023**, *7*, 2300324.
[26] S. Toikkonen, G. K. Grandhi, S. Wang, B. Baydin, B. Al-Anesi, L. K. Jagadamma, P. Vivo, *Adv. Devices Instrum.* **2024**, *5*, 0048.
[27] P. Sánchez-Fernández, C. A. Aranda, R. Escalante, A. J. Riquelme, R. Demadrille, P. Pistor, G. Oskam, J. A. Anta, *Solar RRL* **2024**, *8*, 2400149.
[28] Z. Skafi, J. Xu, V. Mottaghitalab, L. Mivehi, B. Taheri, F. Jafarzadeh, S. K. Podapangi, D. Altamura, M. R. Guascito, L. Barba, C. Giannini, A. Rizzo, F. De Rossi, H. J. Lomeri, L. Sorbello, F. Matteocci, F. Brunetti, T. M. Brown, in *2023 IEEE Nanotechnol. Mater. Devices Conf. NMDC*, IEEE, Paestum, Italy **2023**.
[29] R. Speranza, M. Reina, P. Zaccagnini, A. Pedico, A. Lamberti, *Electrochim. Acta* **2023**, *460*, 142614.
[30] J. I. Kwak, S.-H. Nam, L. Kim, Y.-J. An, *J. Hazard. Mater.* **2020**, *392*, 122297.
[31] N. Mariotti, M. Bonomo, L. Fagiolari, N. Barbero, C. Gerbaldi, F. Bella, C. Barolo, *Green Chem.* **2020**, *22*, 7168.
[32] S. Gressler, F. Part, S. Scherhaufer, G. Obersteiner, M. Huber-Humer, *Sustain. Mater. Technol.* **2022**, *34*, e00501.
[33] E. Buitrago, A. M. Novello, T. Meyer, *Helv. Chim. Acta* **2020**, *103*, e2000074.
[34] A. Ghosh, *Sol. Energy* **2022**, *237*, 213.
[35] M. L. Parisi, S. Maranghi, L. Vesce, A. Sinicropi, A. Di Carlo, R. Basosi, *Renew. Sustain. Energy Rev.* **2020**, *121*, 109703.
[36] K. Miettunen, A. Santasalo-Aarnio, *J. Clean. Prod.* **2021**, *320*, 128743.
[37] G. Spinelli, M. Freitag, I. Benesperi, *Sustain. Energy Fuels* **2023**, *7*, 916.
[38] "PubChem Compound Summary for CID 6342, Acetonitrile," https://pubchem.ncbi.nlm.nih.gov/compound/Acetonitrile (accessed: October, 2024).
[39] A. Ebenezer Anitha, M. Dotter, *Energies* **2023**, *16*, 5129.
[40] J. Capitão, J. Martins, S. Emami, D. Ivanou, A. Mendes, *Sol. Energy* **2023**, *249*, 476.
[41] F. Santos, J. Martins, J. Capitão, S. Emami, D. Ivanou, A. Mendes, *ACS Appl. Energy Mater.* **2022**, *5*, 7220.
[42] R. Speranza, P. Zaccagnini, A. Scalia, E. Tresso, A. Lamberti, *J. Power Sources* **2023**, *583*, 233581.
[43] F. Raffone, A. Lamberti, G. Cicero, *Electrochim. Acta* **2023**, *458*, 142344.
[44] D. Spadaro, J. Barichello, I. Citro, G. Calogero, *Solar* **2023**, *3*, 229.
[45] N. Sangiorgi, A. Sangiorgi, A. Sanson, *J. Electroanal. Chem.* **2022**, *915*, 116352.
[46] F. Bella, L. Porcarelli, D. Mantione, C. Gerbaldi, C. Barolo, M. Grätzel, D. Mecerreyes, *Chem. Sci.* **2020**, *11*, 1485.
[47] S. Domenici, R. Speranza, F. Bella, A. Lamberti, T. Gatti, *Solar RRL* **2025**, *9*, 2400838.
[48] K. S. Teoh, M. Melchiorre, F. A. Kreth, A. Bothe, L. Köps, F. Ruffo, A. Balducci, *ChemSusChem* **2023**, *16*, e202201845.
[49] F. Kerkel, M. Markiewicz, S. Stolte, E. Müller, W. Kunz, *Green Chem.* **2021**, *23*, 2962.
[50] S. Dutta, I. K. M. Yu, D. C. W. Tsang, Y. H. Ng, Y. S. Ok, J. Sherwood, J. H. Clark, *Chem. Eng. J.* **2019**, *372*, 992.
[51] A. Sacco, *Renew. Sustain. Energy Rev.* **2017**, *79*, 814.
[52] Q. Wang, J.-E. Moser, M. Grätzel, *J. Phys. Chem. B* **2005**, *109*, 14945.
[53] F. Fabregat-Santiago, J. Bisquert, G. Garcia-Belmonte, G. Boschloo, A. Hagfeldt, *Sol. Energy Mater. Sol. Cells* **2005**, *87*, 117.
[54] F. Bella, E. D. Ozzello, A. Sacco, S. Bianco, R. Bongiovanni, *Int. J. Hydrog. Energy* **2014**, *39*, 3036.
[55] A. Hauch, A. Georg, *Electrochim. Acta* **2001**, *46*, 3457.
[56] R. Kern, R. Sastrawan, J. Ferber, R. Stangl, J. Luther, *Electrochim. Acta* **2002**, *47*, 4213.
[57] C. Worsley, D. Raptis, S. Meroni, A. Doolin, R. Garcia-Rodriguez, M. Davies, T. Watson, *Energy Technol.* **2021**, *9*, 2100312.
[58] Z. Kebede, S.-E. Lindquist, *Sol. Energy Mater. Sol. Cells* **1999**, *57*, 259.
[59] M. Bonomo, A. D. Carlo, D. Dini, *J. Electrochem. Soc.* **2018**, *165*, H889.
[60] M. Wu, X. Lin, Y. Wang, L. Wang, W. Guo, D. Qi, X. Peng, A. Hagfeldt, M. Grätzel, T. Ma, *J. Am. Chem. Soc.* **2012**, *134*, 3419.
[61] M. Corva, N. Blanc, C. J. Bondue, K. Tschulik, *ACS Catal.* **2022**, *12*, 13805.
[62] P. Khadke, T. Tichter, T. Boettcher, F. Muench, W. Ensinger, C. Roth, *Sci. Rep.* **2021**, *11*, 8974.
[63] B. C. O'Regan, J. R. Durrant, P. M. Sommeling, N. J. Bakker, *J. Phys. Chem. C* **2007**, *111*, 14001.
[64] A. Mashreghi, F. Bahrami Moghadam, *J. Solid State Electrochem.* **2016**, *20*, 1361.
[65] . Masud, H. K. Kim, *ACS Omega* **2023**, *8*, 6139.
[66] J. Wu, Z. Lan, J. Lin, M. Huang, P. Li, *J. Power Sources* **2007**, *173*, 585.
[67] M. Pazoki, U. B. Cappel, E. M. J. Johansson, A. Hagfeldt, G. Boschloo, *Energy Environ. Sci.* **2017**, *10*, 672.
[68] A. Fukui, R. Komiya, R. Yamanaka, A. Islam, L. Han, *Sol. Energy Mater. Sol. Cells* **2006**, *90*, 649.
[69] Z. Yu, N. Vlachopoulos, M. Gorlov, L. Kloo, *Dalton Trans.* **2011**, *40*, 10289.
[70] F. Santos, D. Ivanou, A. Mendes, *Solar RRL* **2024**, *8*, 2300574.
[71] A. Hagfeldt, G. Boschloo, L. Sun, L. Kloo, H. Pettersson, *Chem. Rev.* **2010**, *110*, 6595.
[72] H.-L. Hsu, W.-T. Hsu, J. Leu, *Electrochim. Acta* **2011**, *56*, 5904.
[73] A. Kumar, A. Sharma, B. G. De La Torre, F. Albericio, *Molecules* **2019**, *24*, 4004.
[74] "γ-Valerolactone, 98%, Thermo Scientific Chemicals," https://www.fishersci.no/shop/products/valerolactone-98-thermo-scientific/p-3758968 (accessed: May, 2025).